Combined light and electric response of topographic liquid crystal network surfaces

ADVANCED FUNCTIONAL MATERIALS
www.afm-journal.de

Combined Light and Electric Response of Topographic Liquid Crystal Network Surfaces

*Wei Feng, Dirk J. Broer, and Danqing Liu**

An approach is proposed to create robust liquid crystalline polymer coatings that exhibit sensitivity and dynamic reversibility toward multiple external stimuli including UV irradiation and electrical input. This coating spontaneously alters its surface topographic texture and thickness in response to each of these signals. The corresponding deformations are induced by the photo-/electro-mechanical properties and dielectric anisotropy in the liquid crystal networks through order parameter reduction and anisotropic volume expansions. The deformation proceeds fast within several seconds both for activation and for the relaxation to the initial state upon switching the trigger(s) on and off. Light and electric field can be applied independently to excite the topographies or in a synergistic manner to enhance the deformation amplitude. Upon elimination of the combined light and electric actuating trigger, the relaxation to the initial close to flat state follows a complex pathway. Depending on the elimination order the topographic structure can be rapidly erased or can be kept in a bistable state. The results of this study are relevant for various fields, for instance, switchable controlled friction, controlled adhesion, and release of objects and haptics where they affect human perception both in passive and dynamic manner.

1. Introduction

The structure of a coating surface is of critical importance by its function as the interface between device and its environment.[1–4] Coatings that exhibit a variable surface structure are of special interest as they might change their appearance and contact mechanics, e.g., in response to changes in the environment or by an applied trigger.[5–9] Various stimuli, such as light,[10–15] humidity,[16] heat,[17,18] or electricity[19–21] have been investigated to switch the surface properties and to achieve so-called smart functions. Consequently, by triggered actuation various tasks can be performed, varying from object movement,[11,22,23] self-cleaning,[19,24,25] haptics[26,27] to biomedical[28–31] and microfluidics applications.[32–34] However, despite their already smart behavior, new functionalities and new actuation principles are desired. For instance, the recent developments of soft robotic materials require the combined sensing and acting in a single material.[35] For this reason, a combined sensitivity for different stimuli both in sensing and actuation leads to new pathways for complex functions. For example, light as the trigger imparts a contactless and remote control that can be sensed locally and on distance, while electrical sensitivity allows an easy integration in existing electronic devices to drive the actuation. More importantly, when the stimuli work in concert and interact with each other, more complex responses could be expected.[36,37]

Although there have been some reports about multiple stimuli-responsive polymeric systems (e.g., micelles in solution),[38] these stimuli functioned independently and there was no mutual interaction between them. Therefore, the orchestrated actuation of responsive systems by combining multiple stimuli in a sometimes independent and on-demand controlled interactive way still remains a challenge that we address in this paper in relation to responsive surface mechanics of a modified liquid crystal network (LCN) coating. We have chosen for an LCN coating with a polydomain configuration, fabricated via polymerization of LC monomers from a randomly ordered nematic phase. By incorporating UV-sensitive azobenzene groups and polar LC mesogens in the LCN coating, the LCN is responsive to both UV light and electric fields. By nature, the whole system is also sensitive to temperature variations, which can for instance be indulged by high-frequency electric fields. The LCN domains of different molecular orientation (director) will have a different directional response. In addition, there will be a multifold of domain boundaries and defect structures that are all known to respond to the trigger in their own specific manner with in-plane stresses due to changes in the scalar order parameter and volume expansion due to network oscillations. Of particular interest are the localized responses and their relaxation under different sequences of the respective administration and elimination of light and electricity. Moreover, it is of interest whether the amplitudes of deformation can be enhanced when the two triggers work in concert.

W. Feng, Prof. D. J. Broer, Dr. D. Liu
Laboratory of Stimuli-Responsive Functional Organic Materials & Devices (SFD)
Department of Chemical Engineering and Chemistry
Eindhoven University of Technology
Den Dolech 2, 5612 AZ Eindhoven, The Netherlands
E-mail: d.liu1@tue.nl

W. Feng, Prof. D. J. Broer, Dr. D. Liu
Institute for Complex Molecular Systems (ICMS)
Eindhoven University of Technology
Den Dolech 2, 5612 AZ Eindhoven, The Netherlands

The ORCID identification number(s) for the author(s) of this article can be found under https://doi.org/10.1002/adfm.201901681.

DOI: 10.1002/adfm.201901681

2. Results and Discussion

To show the synergistic effect of UV light and AC electric field, LCN coatings with a polydomain configuration were chosen. They do not require harsh clean-room environment and specific alignment conditions as in monodomain systems, while multiple localized actuation is acquired. In order to achieve multiple sensitivities, the coating composition in **Figure 1**a is applied. The fluorinated dopant **1** induces the formation of multiple domains as its phase separated sub-micron entities act as nucleation centers to break the formation of domains of larger sizes.[12] The azobenzene derivative **2** endows the coating with UV light sensitivity through its *trans–cis* oscillation when exposed with UV light. The LC mesogens (**3** and **5**) with large dipole moment enhance the dielectric permittivity by which they contribute to a more pronounced deformation effect caused by the electric field. Monomer **4** is added to reduce the viscosity of the mixture and to expand on the processing temperature range. The LC mixture exhibits a nematic phase at room temperature, facilitating the fabrication process by spin coating. After spin-coating, the monomer coating is photopolymerized at room temperature with light wavelength >400 nm using a UV cut-off filter. The polarized optical microscope images in Figure 1b reveal multiple, optical retardation related, colors confirming the polydomain configuration of the coating. As a consequence of the local director variations within the domains and the corresponding surface tension gradients, as well the director-dependent polymerization shrinkage, the obtained surfaced is corrugated with surface height differences of the order of 300 nm.

The LCN coating is independently triggered by UV light and AC electric field. For electrical actuation, the 5 µm spaced interdigitated electrodes at the substrate (Figure 1c) provide an in-plane AC electric field. Both UV light and the AC field are known to induce an LC order parameter reduction leading to shear stresses that escape by giving a deformation into the direction orthogonal to the film surface. For UV light, the domains with their orientation in the plane of the film absorb most of the light and their expansion due to the *trans* to *cis* conversion of the azobenzene moieties is into directions orthogonal to the director and the film surface. In contrast the domains where the director is predominantly perpendicular tend to expand universally in the plane of the film and shrink in the direction orthogonal to the film surface. Also, for the alternating electric field, the oscillation of LC mesogens induces the order parameter decrease, either by some dielectric heating or by stress-induced deformation at the main chains, with similar local expansion or contraction, as demonstrated in the uniaxially aligned LCN[20] and LCN with fingerprint configuration.[19] Consequently, the surface deforms in an irregular pattern related to domain sizes, their orientation, and that of the director patterns in their neighboring domains (Figure 1d).[12]

To quantify the topographic deformation of the surface in response to UV light or an AC electric field, we define a modulation amplitude M_a being the maximum height difference between adjacent peaks and valleys divided by the coating thickness.

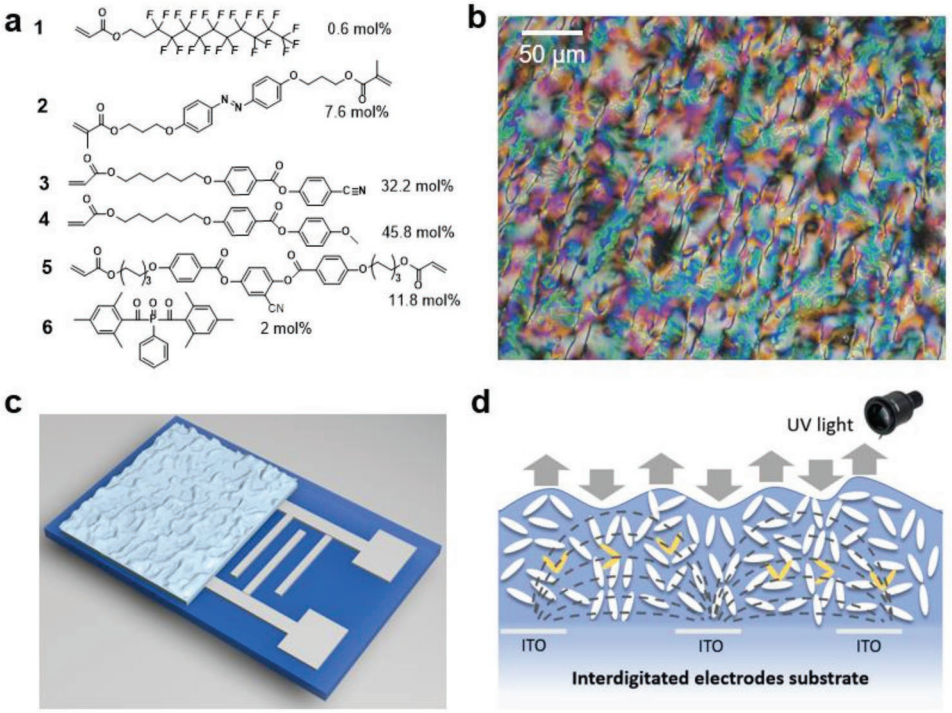

Figure 1. Deformation principle of the multistimuli-responsive coating. a) Chemical composition for fabrication of the polydomain LCN coating. b) Polarized optical microscopic image of a typical polydomain sample. c) Illustration of the LCN coating on interdigitated electrodes. The electrodes on glass are 3 µm wide and the gap between adjacent electrodes is 5 µm. d) Schematic illustration of the topographical deformation when the order parameter is decreased by UV light-induced azobenzene *trans–cis* isomerization and/or an AC electric field.

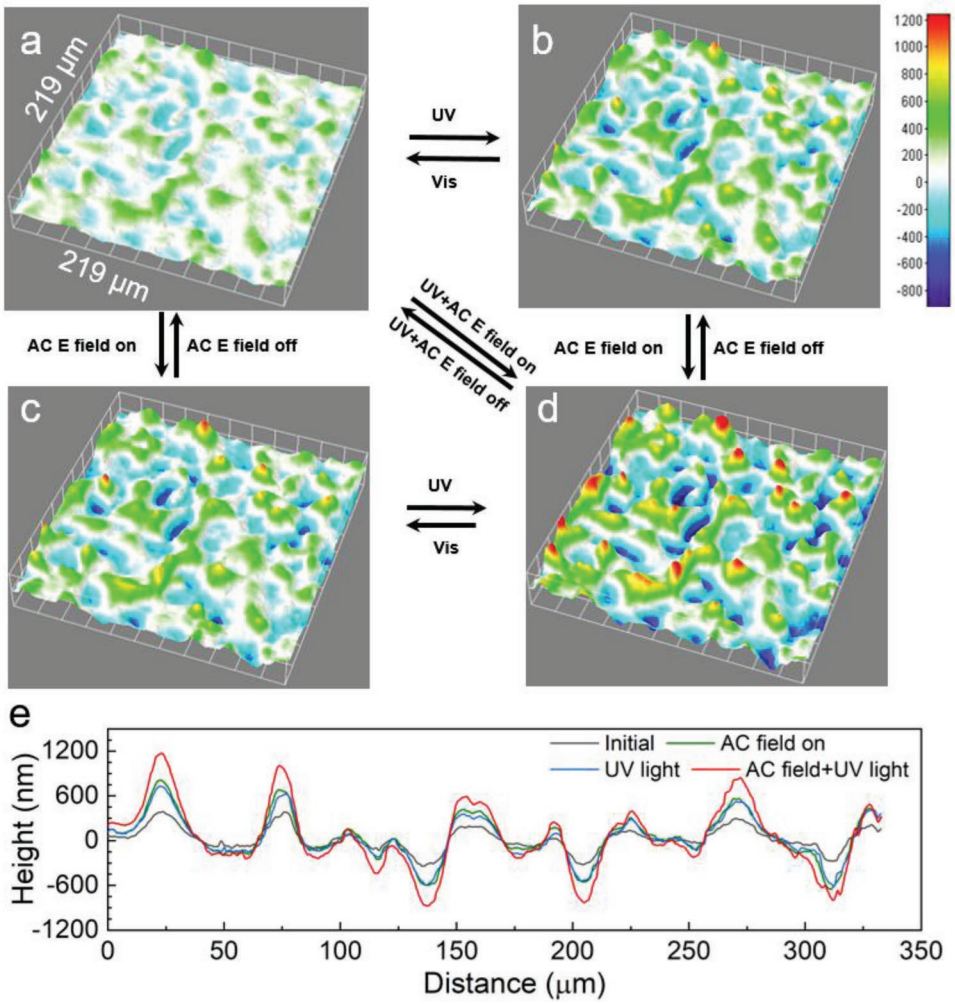

Figure 2. UV light and electric field orthogonally and synergistically actuated surface topographies. 3D images showing the surface topography of a) the initial state at RT, b) during UV illumination, and c) under an AC electric field (16 V_{rms} μm^{-1}, 900 kHz), d) the combines UV illumination and AC field actuation. e) 2D cross-section surface profiles at UV light, electrical actuation, and with both stimuli. The thickness of the coating is 7 µm.

Figure 2 presents the 3D surface topographies and a 2D cross-section under the various actuation principles. When we expose the sample with only UV light (365 nm, 150 mW cm^{-2}) the maximum height difference between valleys and hills reaches a value of ~600 nm. Without light exposure but under an AC electric field (16 V_{rms} μm^{-1}, 900 kHz; optimization is described in the Supporting Information) the maximum height difference is of 680 nm. These values are obtained by subtracting the height values of 25 and 140 µm shown in Figure 2e. For a coating thickness of 7 µm these data correlate to M_a values of 8.6% and 9.7%. When the LCN is simultaneously actuated by the in-plane electric field and UV light, the topographical deformation is enhanced to 1280 nm (M_a = 18.3%), which corresponds to the sum of the deformations with the UV light and AC electric field alone. The enhanced deformation is further characterized by the height distribution histograms: the narrow histogram of the initial state (**Figure 3**a) indicates a relatively initial flat surface, the distribution increases in width by light or AC field (Figure 3b,c), and has the widest distribution histogram when simultaneously actuated by UV light and AC electric field (Figure 3d).

A remarkable aspect is that the deformation by light and by electricity occurs at exactly the same position and that this position overlaps with the initial surface topography prior to actuation. This becomes nicely obvious in Figure 2 where the initial hills are becoming higher and the valleys become lower. A possible explanation can be found by analyzing the origin of the initial topographical defects. When the films are being photopolymerized they are subjected to polymerization shrinkage. The volume shrinkage of these materials can be easily as high as 4%.[39] In isotropic acrylate coatings this is not well visible as the shrinkage occurs uniformly over the whole surface, as is also the case for anisotropic films with a uniform alignment. However, in our case we have domains of locally different alignment and it is known that shrinkage is anisotropic with the highest shrinkage value parallel to the director.[39] This would mean that the orientation at the topographic hills is planar and at the valleys homeotropic. This is further confirmed by birefringence measurements. Upon reducing the order parameter, either by light, by an electrical field, or by temperature, the planar area will expand and the homeotropic area will shrink,

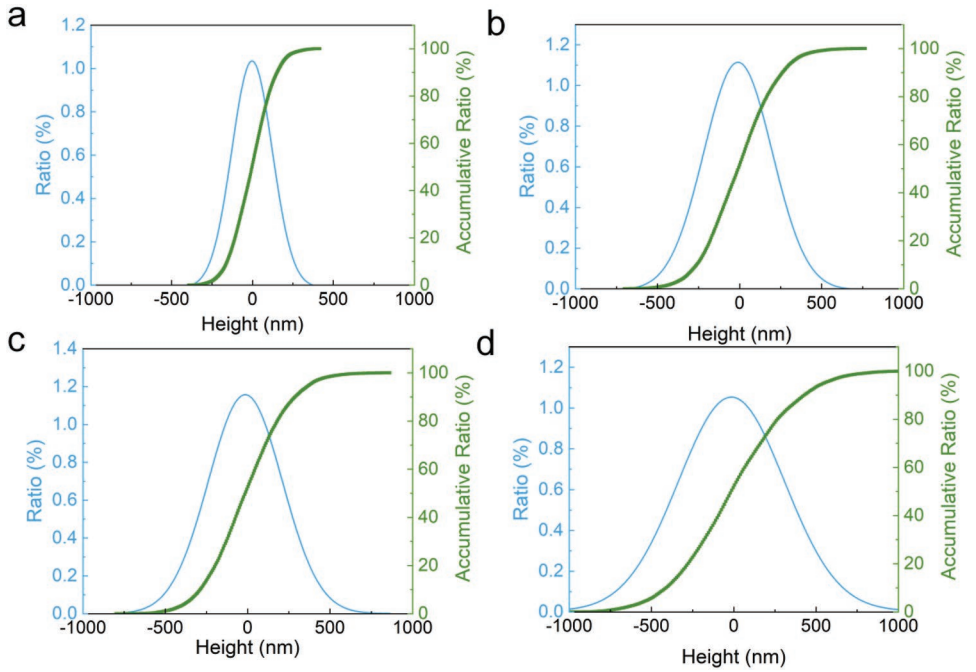

Figure 3. Height distribution histograms of different states: a) initial unactuated state, b) UV actuated state, c) AC electrically actuated state, and d) the combined UV and AC electrically actuated state.

thus amplifying the initial surface structure as shown in Figure 2b–d.

In recent publications it became clear that upon actuation by light and by electrical fields the influence of temperature cannot be ignored.[21,40] Light heats up the sample by absorption of the azobenzene moieties. The relatively high-frequency electrical field leads to dielectric heating when the dipoles try to team up with the alternating polarization of the field. This might lead to the conclusion that we are predominantly looking to temperature-induced surface deformation rather than photochemical dipolar effects. To bring this into perspective, we mapped the various influences by in situ measuring the temperature under the various conditions. This is summarized in the Supporting Information. The conclusion is that under our illumination conditions the temperature is increased by only 2 °C corresponding to negligible topographical deformation. The heating is less than normally measured in free-standing films which is attributed to the small thicknesses of the film (7 µm) and the glass substrate acting as heat sink. The temperature increment by dielectric heating effect is measured to be 50 °C. Heating the sample on a hot stage to 70 °C gives an M_a value of 3.1% (Figure S2, Supporting Information). This is smaller than the M_a of 9.7% we measured the electrically actuated surface but it shows that in this case thermal effects as induced by the AC field cannot be ignored.

In our dual-stimulus-responsive system, UV light and AC electric field address the same domains in the same manner and add up when they are applied simultaneously. The 3D view, POM image, and the deformation amplitude of each domain are shown in **Figure 4**a,b, respectively. The deformation amplitudes of the various domains (Figure 4c) are subtracted using the initial topography and the topography of the combined UV and AC field actuated state. To investigate the deformation kinetics, we selected two domains with the largest deformation amplitude to monitor their height change in time. The birefringence of domain 1 is measured with a Berek compensator to be 0.030 that indicates a near-homeotropic alignment with a small off-axis tilt from the normal, whereas domain 2 has a birefringence of 0.134 that indicates a near-planar alignment with a small tilt angle from the in-plane axes.[41] The synergistic effect of two stimuli is accompanied by the consecutive reduction of order parameter ***S***, indicated by the birefringence change: the birefringence of the LCN coating with uniform planar alignment decreases from 0.134 to 0.119 with UV illumination alone, to 0.116 with AC electric field actuation alone, and to 0.096 with both stimuli (Figure S5, Supporting Information). Time-resolved deformation monitoring of two domains indicates that the deformation amplitudes actuated by UV light and electric field simply add up under the conditions chosen (Figure 4d–f), which is rarely reported in other stimuli-responsive systems.[38] In the process of relaxation upon removal of the stimuli, the deformation behavior of the coating depends strongly on the order in which each stimulus is removed. If the UV light is removed while the AC field is still on, the deformation caused by the UV decays rapidly and there is no residual deformation after also the electrical is switched off, as shown in Figure 4d,g. In contrast, when the UV light is switched off in the absence of the AC field, there will be a large residual deformation (Figure 4e–g), due to the relatively slow thermal relaxation rate of the *cis*-azobenzene. However, we found that when during this process of slow relaxation the AC field is switched on that it will rapidly erase the UV-induced residual deformation. To elucidate these phenomena, we performed UV–vis studies on the conversion of the azobenzene moieties in the LCN coatings. **Figure 5**a shows the absorption of the azobenzene, as

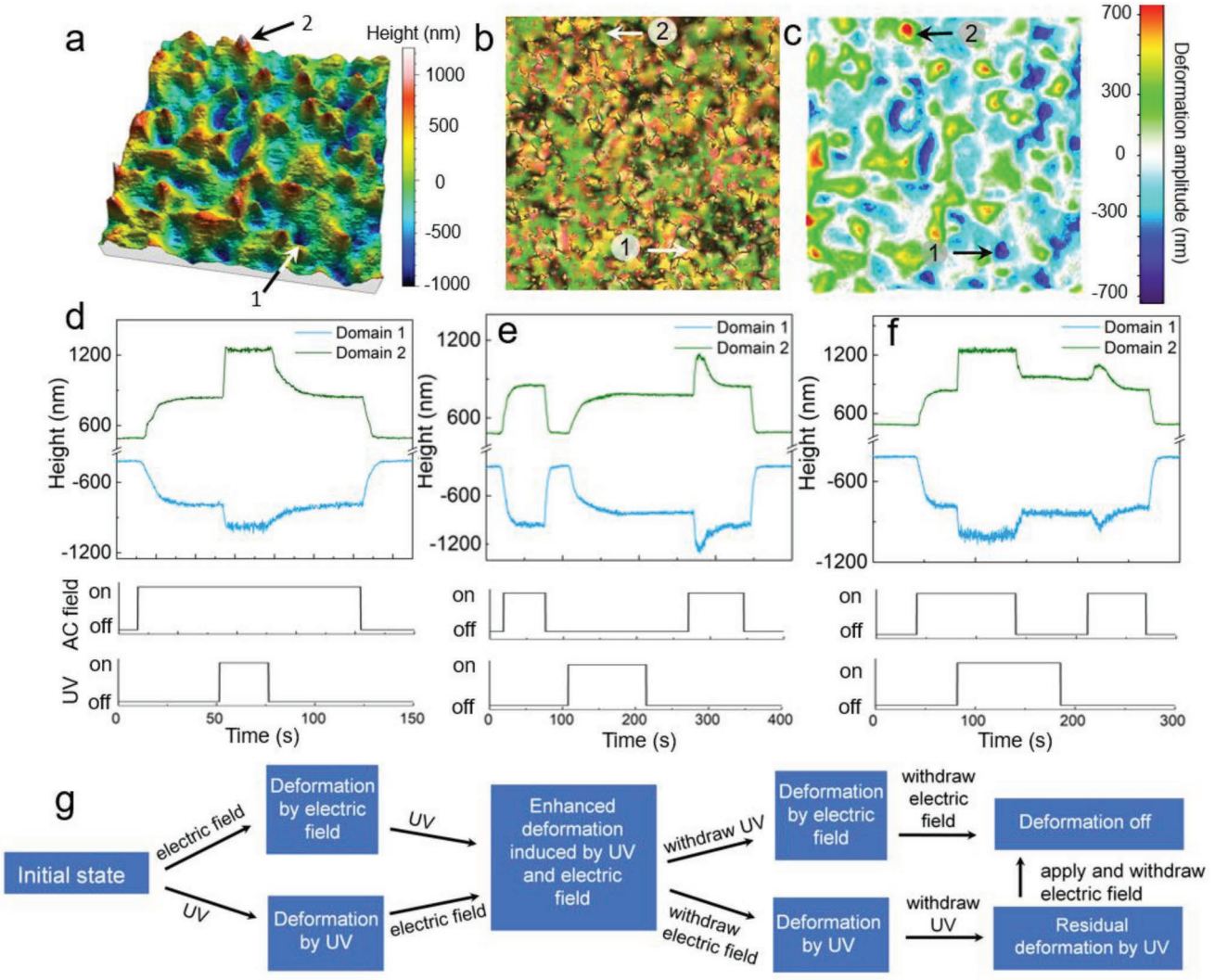

Figure 4. Formation and relaxation of the surface topographies as a function of the actuation sequence as monitored at a near-planar and a near homeotropic domain. a) 3D view of the surface topographies of the analyzed area. b) Polarized microscopic image prior to actuation with an indication of the location of the planar (1) and homeotropic (2) domain. c) Deformation amplitudes of the same area under UV/AC field actuation. d–f) Set of different sequences of UV and AC field actuation and the influence of the sequence of their elimination on the relaxation. g) Illustrative scheme of the actuation and stimuli withdrawal processes. The deformation behavior depends on the elimination order of the stimuli.

incorporated in our LCN, in the photostationary dark state and momentarily after UV irradiation. Figure 5b correlates the rate of conversion of the azobenzene as indicated by the absorption band measured at 365 nm with the relaxation process zoomed in at the location of the actuated hills and valleys after switching off the UV light in the presence of the AC field. By comparing the electricity-induced *cis–trans* isomerization kinetics with that caused by purely thermal effect when heated to the similar temperature (Figure 5c) in the absence of the AC field, these two isomerization rates correlate well with each other in Figure 5d, indicating that the *cis–trans* isomerization is induced by the electrothermal effect. We also considered the impact of the dielectric constant difference of polar azobenzene *cis*- and the *trans*-isomer on the electromechanical performance of LCN, and little difference of the dielectric anisotropy was found before and after azobenzene *trans–cis* isomerization (Figure S6, Supporting Information).

In order to correlate the sub-micrometer level surface deformation to macroscopic properties, the static friction coefficient μs of two actuated surfaces sliding along each other was measured under the various actuation conditions (see Figure S7, Supporting Information). With the static friction coefficient defined as $\mu_s = \tan \theta_c$, in which θ_c is the critical sliding angle at which the glass plates starts sliding from the position of rest, the μ_s of different actuation states is determined. In the absence of any of the stimuli $\mu_s = 0.58$. When the AC electric field is switched on $\mu_s = 1.28$ as the result of the increased surface roughness and interlocking of the protruded structures. A similar value was found with UV light switched on: $\mu_s = 1.23$, while with both AC E field and UV light $\mu_s = 11.43$. This result confirms the results of the topographical measurements from which it was concluded that light and AC field gives a close to similar topographical change that becomes attenuated of both actuation sources are switched on simultaneously.

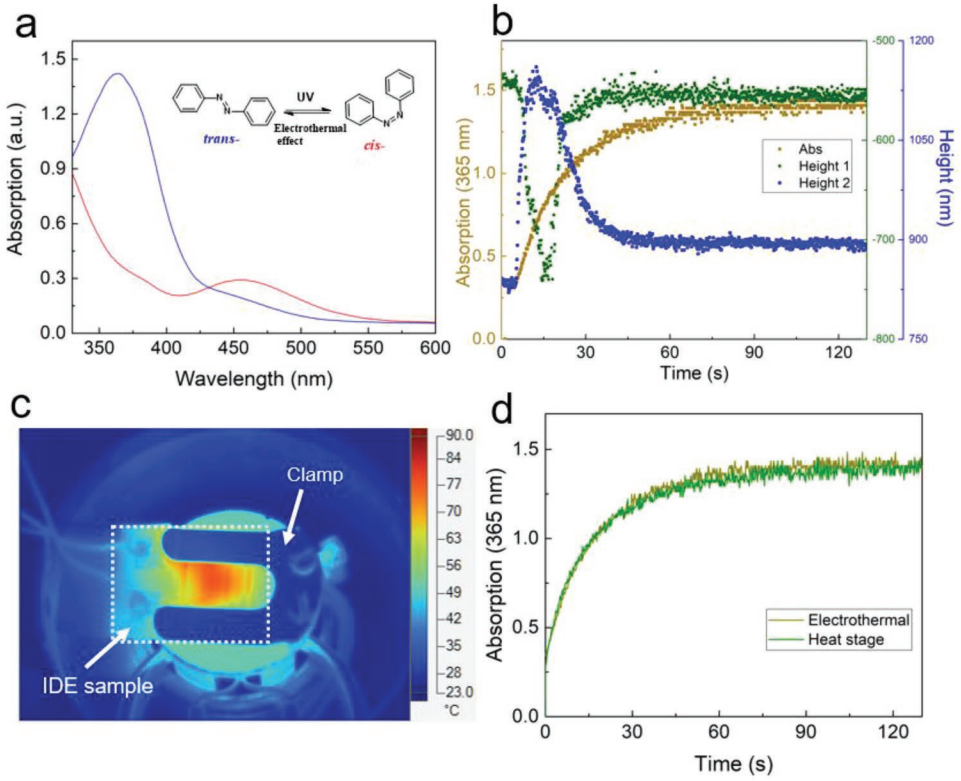

Figure 5. a) UV–vis spectra of LCN containing *trans*- and *cis*-azobenzene groups. b) Correlation between *cis*–*trans* azobenzene isomerization kinetics and topographical deformation kinetics. The topographical deformation was locally measured with digital holographic microscopy while the UV–vis measurement was conducted integrated over the surface area with a photospectrometer. c) Sample temperature image when actuated with AC electric field. d) Investigation of *cis*–*trans* isomerization kinetics of azobenzene groups when triggered by electrothermal effect and the same temperature provided via a hot plate.

In conclusion, combining light and electricity-responsive properties of liquid crystal polymer networks, we demonstrated orthogonal and synergistic switch of the LCN coating topography in response to UV light and AC electric field. When actuated, the deformation by one trigger can be enhanced by the other one. In the stimulus withdrawal process, the deformation behaviors depend on the withdrawal order of the stimuli, surpassing a simplistic on/off binary switching mode compared with conventional multiresponsive polymers. This strategy enables the integration of two independent stimuli (UV light and electric field) into elaborate dynamic actuation and complex functions in which, on demand, the bistability of the surface structure, manifested as for instance a change in friction coefficient, can be switched on and off or can be maintained in the absence of a trigger until erased by a short AC field trigger event.

3. Experimental Section

Materials: Fluorinated monomer 1 was purchased from Sigma–Aldrich. Photoresponsive monomer 2 was obtained from Syncom (Groningen). Liquid crystal monomers 3 and 4 were obtained from Merck. Monomer 5 was supplied by Phillips Research Laboratories. Photoinitiator 6 was provided by Ciba Specialty Chemicals.

Sample Preparation: The substrates with interdigitated electrodes were cleaned with sonication in acetone and isopropanol for 5 min, respectively, and then subjected to UV ozone for 20 min. The substrates were then treated with methacryloxypropyltrimethoxysilane (silane A174) using dip coating to promote the adhesion of polymer to the glass substrate. The liquid crystal monomer dissolved in THF (25 wt%) was spin-coated on the substrate at 1000 rpm for 30 s (acceleration rate 50 rpm s^{-1}). Afterward, photo-initiated polymerization was conducted in a nitrogen atmosphere by exposure with a mercury lamp (Omnicure EXFO S2000) at 36 °C for 40 min and a postcure at 120 °C for 10 min. A cut-off filter (light wavelength >400 nm) was placed between the light source and sample to avoid the *trans*–*cis* isomerization of azobenzene groups during polymerization.

Characterization: The thickness of the coating was measured with an interferometer (Fogal Nanotech Zoomsurf). The polydomain configuration was checked by crossed polarizer integrated in an optical microscope (Leica DM2700). The dynamic surface topographies were characterized with the Digital Holographic Microscope (Lyncée Tec). LED lamps (Thorlabs, M365L2) were used to provide monochromatic UV light. The AC electric field with sinusoidal wave function was provided by a function generator (Tektronix AFG3252C) and amplified by an amplifier (Falco Systems WMA-300) while measured with an oscilloscope (Keysight Infinii Vision DSO-X 3032T).

The height distribution was obtained from the surface topography images by calculating the portion of pixels of every height to the total pixel number of the whole image, and the accumulative ratio was obtained by accumulatively summing up the ratio of every height.

Supporting Information

Supporting Information is available from the Wiley Online Library or from the author.

Acknowledgements

This work was supported by European Research Council with the ERC Advanced Grant 66999 (VIBRATE), the framework of the 4TU.High Tech Materials research program "New Horizons in designer materials," NWO VENI grant 15135. Merck is acknowledged for providing ITO IDE. The authors acknowledge Prof. Michael Wübbenhorst and Alessia Gennaro at KU Leuven for dielectric anisotropy measurement.

Conflict of Interest

The authors declare no conflict of interest.

Keywords

dual-responsive, dynamic surface topographies, electricity, light, liquid crystal networks

Received: February 25, 2019
Revised: April 8, 2019
Published online: April 26, 2019

[1] W. Barthlott, C. Neinhuis, *Planta* **1997**, *202*, 1.
[2] T.-S. Wong, S. H. Kang, S. K. Y. Tang, E. J. Smythe, B. D. Hatton, A. Grinthal, J. Aizenberg, *Nature* **2011**, *477*, 443.
[3] Z. Wang, Y. Liu, P. Guo, L. Heng, L. Jiang, *Adv. Funct. Mater.* **2018**, *28*, 1801310.
[4] E. Kizilkan, J. Strueben, A. Staubitz, S. N. Gorb, *Sci. Robot.* **2017**, *2*, eaak9454.
[5] R. Vaia, J. Baur, *Science* **2008**, *319*, 420.
[6] H. Kuroki, I. Tokarev, S. Minko, *Annu. Rev. Mater. Res.* **2012**, *42*, 343.
[7] F. Xia, L. Jiang, *Adv. Mater.* **2008**, *20*, 2842.
[8] P. Irajizad, M. Hasnain, N. Farokhnia, S. M. Sajadi, H. Ghasemi, *Nat. Commun.* **2016**, *7*, 13395.
[9] W. Wang, J. V. I. Timonen, A. Carlson, D.-M. Drotlef, C. T. Zhang, S. Kolle, A. Grinthal, T.-S. Wong, B. Hatton, S. H. Kang, S. Kennedy, J. Chi, R. T. Blough, M. Sitti, L. Mahadevan, J. Aizenberg, *Nature* **2018**, *559*, 77.
[10] R. Wang, K. Hashimoto, A. Fujishima, M. Chikuni, E. Kojima, A. Kitamura, M. Shimohigoshi, T. Watanabe, *Nature* **1997**, *388*, 431.
[11] J.-A. Lv, Y. Liu, J. Wei, E. Chen, L. Qin, Y. Yu, *Nature* **2016**, *537*, 179.
[12] D. Liu, L. Liu, P. R. Onck, D. J. Broer, P. Palffy-Muhoray, *Proc. Natl. Acad. Sci. USA* **2015**, *112*, 3880.
[13] M. E. McConney, A. Martinez, V. P. Tondiglia, K. M. Lee, D. Langley, I. I. Smalyukh, T. J. White, *Adv. Mater.* **2013**, *25*, 5880.
[14] H. K. Bisoyi, Q. Li, *Chem. Rev.* **2016**, *116*, 15089.
[15] L. Wang, Q. Li, *Chem. Soc. Rev.* **2018**, *47*, 1044.
[16] S. Zeng, R. Li, S. G. Freire, V. M. M. Garbellotto, E. Y. Huang, A. T. Smith, C. Hu, W. R. T. Tait, Z. Bian, G. Zheng, D. Zhang, L. Sun, *Adv. Mater.* **2017**, *29*, 1700828.
[17] T. H. Ware, M. E. McConney, J. J. Wie, V. P. Tondiglia, T. J. White, *Science* **2015**, *347*, 982.
[18] H. Hou, J. Yin, X. Jiang, *Adv. Mater.* **2016**, *28*, 9126.
[19] W. Feng, D. J. Broer, D. Liu, *Adv. Mater.* **2018**, *30*, 1704970.
[20] D. Liu, N. B. Tito, D. J. Broer, *Nat. Commun.* **2017**, *8*, 1526.
[21] C. Wang, K. Sim, J. Chen, H. Kim, Z. Rao, Y. Li, W. Chen, J. Song, R. Verduzco, C. Yu, *Adv. Mater.* **2018**, *30*, 1706695.
[22] R. Eelkema, M. M. Pollard, J. Vicario, N. Katsonis, B. S. Ramon, C. W. M. Bastiaansen, D. J. Broer, B. L. Feringa, *Nature* **2006**, *440*, 163.
[23] Z. Yang, J. K. Park, S. Kim, *Small* **2018**, *14*, 1702839.
[24] T. Guo, P. Che, L. Heng, L. Fan, L. Jiang, *Adv. Mater.* **2016**, *28*, 6999.
[25] Y. Lu, S. Sathasivam, J. Song, C. R. Crick, C. J. Carmalt, I. P. Parkin, *Science* **2015**, *347*, 1132.
[26] S. Yim, S. Jeon, S. Choi, *IEEE Trans. Haptics* **2015**, *8*, 90.
[27] K. Jun, J. Kim, I.-K. Oh, *Small* **2018**, *14*, 1801603.
[28] H. Jeon, S. Koo, W. M. Reese, P. Loskill, C. P. Grigoropoulos, K. E. Healy, *Nat. Mater.* **2015**, *14*, 918.
[29] T. Heydari, M. Heidari, O. Mashinchian, M. Wojcik, K. Xu, M. J. Dalby, M. Mahmoudi, M. R. Ejtehadi, *ACS Nano* **2017**, *11*, 9084.
[30] K. Yang, H. Jung, H.-R. Lee, J. S. Lee, S. R. Kim, K. Y. Song, E. Cheong, J. Bang, S. G. Im, S.-W. Cho, *ACS Nano* **2014**, *8*, 7809.
[31] G. Kocer, J. ter Schiphorst, M. Hendrikx, H. G. Kassa, P. Leclere, A. Schenning, P. Jonkheijm, *Adv. Mater.* **2017**, *29*, 1606407.
[32] P. Kant, A. L. Hazel, M. Dowling, A. B. Thompson, A. Juel, *Phys. Rev. Fluids* **2017**, *2*, 094002.
[33] H. R. Holmes, K. F. Böhringer, *Microsyst. Nanoeng.* **2015**, *1*, 15022.
[34] J. ter Schiphorst, J. Saez, D. Diamond, F. Benito-Lopez, A. P. H. J. Schenning, *Lab Chip* **2018**, *18*, 699.
[35] S. A. Morin, R. F. Shepherd, S. W. Kwok, A. A. Stokes, A. Nemiroski, G. M. Whitesides, *Science* **2012**, *337*, 828.
[36] O. M. Wani, R. Verpaalen, H. Zeng, A. Priimagi, A. P. H. J. Schenning, *Adv. Mater.* **2019**, *31*, 1805985.
[37] Z. G. Zheng, R. S. Zola, H. K. Bisoyi, L. Wang, Y. Li, T. J. Bunning, Q. Li, *Adv. Mater.* **2017**, *29*, 1701903.
[38] J. Dong, Y. Wang, J. Zhang, X. Zhan, S. Zhu, H. Yang, G. Wang, *Soft Matter* **2013**, *9*, 370.
[39] R. A. M. Hikmet, B. H. Zwerver, D. J. Broer, *Polymer* **1992**, *33*, 89.
[40] A. H. Gelebart, G. Vantomme, E. W. Meijer, D. J. Broer, *Adv. Mater.* **2017**, *29*, 1606712.
[41] M. Hendrikx, A. P. H. J. Schenning, D. J. Broer, *Soft Matter* **2017**, *13*, 4321.